Journal of the Serbian Chemical Society
JSCS@tmf.bg.ac.rs • www.shd.org.rs/JSCS

J. Serb. Chem. Soc. 91 (0) 1–16 (2026)
JSCS–13509

Original scientific paper
Published 8 Feb 2026

Molecular dynamics-based methodological approach to clarify perfluorooctanoic acid binding on human serum albumin

ALEKSANDRA M. ĐURĐEVIĆ ĐELMAŠ[1], DANILO P. TRAJKOVIĆ[1], KARLA MILČIĆ[2] and MILOŠ K. MILČIĆ[1]*

[1]*University of Belgrade – Faculty of Chemistry, Studentski trg 12–16, 11158 Belgrade, Serbia and* [2]*Institute of Chemistry, Technology and Metallurgy, Department of Chemistry, University of Belgrade, National Institute of the Republic of Serbia, Njegoševa 12, 11000 Belgrade, Serbia*

(Received 20 August, revised 27 August, accepted 5 September 2025)

Abstract: Perfluorooctanoic acid (PFOA) is a persistent environmental contaminant that binds strongly to human serum albumin (HSA), influencing its distribution and toxicokinetics. While crystallographic studies in the presence of myristic acid have identified a limited number of high-affinity binding sites, additional sites may remain undetected due to competitive binding. Here, we combined molecular docking with extensive molecular dynamics (MD) simulations to comprehensively characterize PFOA–HSA interactions. A tiled docking approach revealed twelve non-overlapping binding poses, including six not previously reported. Ligand–residue interaction mapping, *RMSD* analysis and MM/PBSA free energy calculations identified four sites, FA3, FA1, FA4 and FA6, as the most stable PFOA binding positions in the absence of competing ligands. Among all examined sites, FA3 displayed the most favorable calculated binding energy. Furthermore, ligands at both FA1 and FA3 sites exhibited over 23 and 85 kJ/mol more favorable binding energy, respectively as calculated by MM/PBSA, than the ligand at well-characterized FA4 site under other ligand-free conditions. Persistent salt bridges, hydrogen bonds, and halogen contacts were identified as key stabilizing interactions. Free-energy landscapes further confirmed the stability of PFOA binding at these sites. These findings provide a more complete understanding of the PFOA binding landscape on HSA, offering insights that may inform the design of biomimetic capture agents and strategies for environmental remediation.

Keywords: protein–ligand interactions; PFAS; binding free energy calculations.

* Correspondence E-mail: mmilcic@chem.bg.ac.rs
https://doi.org/10.2298/JSC250820067D

INTRODUCTION

Proteins are highly dynamic macromolecules involved in a wide range of vital biological processes both within and between cells. One of their essential functions is transporting various molecules, ranging from simple ions and small gases to more complex compounds such as hormones, fatty acids, neurotransmitters, amino acids, nucleic acids and drugs, collectively referred to as ligands.[1] The interactions between proteins and ligands have been extensively investigated, as proteins are not only capable of reversible ligand binding but often exhibit enzymatic activity that enables ligand transformation.[2] To understand a protein's role at the molecular level, it is crucial to identify its ligand binding site and the specific amino acid residues involved in the interaction. These residues are central to determining binding specificity and are particularly important in enzymatic recognition, where factors like side chain orientation and physicochemical properties critically affect affinity and selectivity.[3] Interestingly, Kuntz *et al.* observed that binding affinity generally increases with ligand size, but this trend plateaus when ligands exceed approximately 15 non-hydrogen atoms. Beyond this threshold, additional atoms contribute minimally to binding energy, revealing a nonlinear relationship between ligand size and binding strength.[4] Consequently, understanding ligand binding involves more than locating the binding site, it requires evaluating the broader molecular and energetic environment that governs the interaction.[5,6] Such insights are indispensable not only for fundamental biological research but also for practical applications such as rational drug design, enzyme optimization, and targeted mutagenesis.[7]

Human serum albumin (HSA) is the most abundant carrier protein in the human body, playing a vital role in maintaining osmotic pressure and transporting a wide variety of endogenous and exogenous ligands (fatty acids, amino acids, hormones, ions such as Ca^{2+}, Na^{+} and K^{+}, water, drugs,…).[8,9] It has been demonstrated that HSA is the principal transporter of perfluorooctanoic acid (PFOA) in the bloodstream.[10] PFOA (C8) is a widely prevalent perfluorinated compound structurally similar to fatty acids, whose exceptional chemical stability and resistance to degradation cause it to persist in the environment and accumulate in living organisms, resulting in significant human exposure through contaminated food and water and raising serious health concerns due to its biological half-life of approximately three years.[11,12]

Experimental and theoretical studies have identified multiple potential PFOA binding sites on HSA.[13–16] Docking simulations have revealed several putative binding locations, suggesting that while docking is a useful tool for predicting interaction sites, it may not fully capture the complexity of ligand binding due to inherent biases and its static nature. Moreover, docking often relies on X-ray crystallographic structures of proteins, which may be incomplete or lack sufficient resolution, further limiting the reliability of this method in accurately identifying true

binding sites. Limited by incomplete molecular models and scoring function shortcomings, docking alone cannot reliably predict binding affinity or the precise binding locations.[17] Protein–ligand association can be described as diffusion across a multidimensional energy landscape, which typically contains an energy minimum corresponding to the bound complex. As the ligand approaches the protein, long-range electrostatic interactions guide the process along a binding funnel that may contain local minima and multiple competing pathways.[18] In the case of PFOA binding to HSA, such complexity is particularly relevant, as this ligand is highly flexible and amphiphilic, capable of transiently interacting with several regions on the protein surface. These dynamic features often elude static docking approaches, which oversimplify the energy landscape and may miss alternative or transient binding modes.

A recent study by Maso *et al.*[13] identified a single high-affinity binding site for PFOA on HSA, along with three lower-affinity sites. These four sites were confirmed through crystallization of HSA with PFOA; however, the experiments were performed in the presence of myristic acid. Consequently, only binding positions where PFOA outcompeted myristic acid were detected, potentially leaving additional PFOA binding sites unidentified. Comprehensive mapping of all binding sites is important for fully understanding PFOA–HSA interactions, as this knowledge would enable the rational design of biomimetics capable of targeting and binding multiple PFOA molecules under diverse environmental conditions. Moreover, identifying all sites could support the development of more robust environmental remediation strategies, producing biomimetics with greater versatility in recognizing and sequestering PFOA across a range of concentrations.

Despite increasing evidence that PFOA can interact with multiple regions of HSA, the complete landscape of binding sites, their relative affinities, and the molecular determinants of binding remain insufficiently characterized. Existing structural studies have been limited by the presence of competing ligands, while computational docking alone cannot capture the conformational flexibility and dynamic nature of ligand–protein interactions. To overcome these limitations, we combined exhaustive molecular docking with molecular dynamics (MD) simulations to evaluate the stability, energetics and residue-level interactions of PFOA at all predicted binding positions. This integrated approach enabled the identification of energetically and kinetically favorable sites under other ligand-free conditions, providing a more comprehensive understanding of the PFOA–HSA interaction network. By mapping these sites and characterizing their key stabilizing interactions, our study offers new insights into the molecular basis of PFOA binding that can inform the design of selective biomimetic capture agents and guide the development of effective environmental remediation strategies.

EXPERIMENTAL

Molecular docking

Although numerous crystal structures of human serum albumin (HSA) are available in the Protein Data Bank, the structure with PDB ID: 1N5U[25] (1.90 Å) was selected for this study due to its high resolution, complete domain coverage, and absence of large conformational distortions, making it a reliable and structurally representative model. Prior to docking, all co-crystallized ligands (*e.g.*, myristic acid) were removed. Protonation states of titratable residues were assigned using H++ 3.0.[19] AutoDockTools[20] (v1.5.7) was used for assigning partial charges to protein atoms. The geometry of anion of perfluorooctanoic acid (PFOA) was optimized at the DFT/B3LYP/6-311G(d,p) level using Gaussian 09.[21] A systematic grid-based search strategy was employed, generating 1,248 partially overlapping boxes (24×24×24 $Å^3$) shifted by 8 Å to ensure complete screening of protein surface and volume. All atoms in the protein molecule were kept rigid, while free rotation around single bonds in ligand were allowed. Docking simulations were performed with AutoDock Vina.[22] Final binding poses and interaction sites were visualized using PyMOL2 and Discovery Studio 2024.

Molecular dynamics simulations

Molecular dynamics (MD) simulations were performed using the AMBER software. The protein structure was prepared by assigning appropriate protonation states and parameterizing it using the ff19SB force field.[23] The DFT-optimized structure of PFOA was used as input, while ligand topologies were generated following the standard procedure recommended by the AMBER developers. For bonds, valence angles, torsion and improper torsion angles and Lennard-Jones parameters standard generalized AMBER force-field version 2 (gaff2) parameters were used.[24] Partial atomic charges were determined by first calculating Mertz–Kollman electrostatic potential at MP2/def2-TZVP level of theory and then deriving partial charges with RESP procedure.[25] Molecular dynamic simulations were performed with 12 ligands simultaneously. Initial ligand positions were determined by docking: 12 poses with the highest docking score were used.

The optimal point charge (OPC) model was used for water and counterions added to neutralize the system. The OPC model was chosen because it provides improved accuracy in reproducing key thermodynamic and dynamic properties of liquid water compared to commonly used three-point and four-point models, while remaining computationally efficient for large-scale MD simulations. The system was neutralized with Na^+ and solvated in a truncated octahedron box of water with at least 10 Å between box edges and protein residues. Additional Na^+ and Cl^- were added to simulate the 0.15 M salt concentration. Simulations were done under periodic boundary conditions and particle mesh evald summation method was used for calculating long range electrostatics. The system was initially minimized for 2,000 steps using Newton–Raphson algorithm, and then slowly heated from 100 to 298 K for 1 ns with time-step of 1 fs, while keeping the volume constant. The initial restraint on protein and ligand atoms was 418.40 kJ/(mol $Å^2$). Next, the system was relaxed for a total of 6 ns with 1 fs time step, in NPT ensemble, by slowly lifting restraints (to 41.64, 4.18 and 0.42 kJ/(mol $Å^2$)). Finally, 5 ns of equilibration in the NPT ensemble with 1 fs time step and no restraints was conducted. For a 1000-ns production run, NPT ensemble was chosen with Langevin thermostat and Berendsen barostat and 2 fs time step. The SHAKE algorithm was employed to impose constraints on hydrogen atoms. Simulations were performed in triplicate starting from the same docking poses but with different randomly assigned initial velocities.

Molecular dynamics trajectory analysis and collective variable calculations were done with the cpptraj program.[26] Gromacs sham utility[27] was used for free energy landscape calculations. PLIP (protein ligand interaction profiler) program was used for calculating protein ligand interactions from MD trajectory. Images are created in Pymol, VMD and Discovery studio visualizer programs.

RESULTS AND DISCUSSION

To identify all potential PFOA binding sites on HSA, we performed molecular docking simulations using the DFT-optimized structure of PFOA and the crystal structure of HSA (PDB ID: 1N5U). To provide structural context, Fig. S-1 of the Supplementary material to this paper illustrates the domain organization of HSA together with its fatty acid binding sites. To achieve exhaustive spatial coverage of the protein surface and internal cavities, the HSA structure was divided into over 1,200 partially overlapping grid boxes. Separate docking calculations were performed for each box using AutoDock Vina, an approach that enables high-resolution, tiled screening and has proven effective for mapping ligand binding to large proteins.[28] This systematic search identified 12 non-overlapping binding poses, with predicted binding scores ranging from –41.00 to –25.94 kJ/mol (Table I, Fig. 1). The top 12 docking poses were selected based on an energy cut-off of 15 kJ/mol relative to the best-scoring pose.

TABLE I. Twelve best-docked PFOA ligands to HSA, labeled as L1-L12, along with their predicted binding energies obtained from molecular docking and calculated binding energies using the MM-PBSA method (kJ/mol). Bolded values indicate 4 ligand binding sites selected after MD simulations

Ligand position	Binding energies estimated by molecular docking	Binding energies calculated by MM-PBSA
L1 (FA5)	–41.00	–34.81±2.09
L2	–37.66	–33.58±4.31
L3	–36.82	–63.89±4.56
L4	–35.98	–87.11±5.82
L5	–35.15	–42.38±5.77
L6	–33.47	–9.16±3.64
L7	–32.22	–6.32±2.38
L8	–30.54	–149.08±3.22
L9	–28.45	–24.31±2.26
L10	–27.20	4.35±1.76
L11	–26.78	–1.26±6.86
L12	–25.94	–14.31±1.92

The docking simulations identified the highest-affinity PFOA binding pose (–41.00 kJ/mol) in fatty acid site 5 (FA5, Fig. S-1), stabilized by multiple non-covalent interactions. Halogen interactions occur between fluorine atoms on the PFOA tail and the side chains of Lys525 and Ala528. The carboxylate head group of PFOA forms a hydrogen bond with Ser579, while carbon–hydrogen bonds are

established with the side chains of Met548 and Leu529. Additional stabilization is provided by a π-lone pair interaction between Phe551 and a fluorine atom, as well as a π-alkyl interaction between Phe551 and the terminal carbon of PFOA. An alkyl interaction is also observed between Lys525 and the terminal carbon of PFOA (Fig. 1, L1). Notably, Met548 has previously been implicated in PFOA binding by Wu *et al.*,[29] although no other interacting residues were reported. Consequently, it remains unclear whether the site described by Wu *et al.* overlaps with the FA5 site identified in this study. Furthermore, crystallographic analysis of HSA in the presence of both myristic acid and PFOA showed myristic acid[13] occupying FA5, suggesting that competitive binding could influence the detection and characterization of this site.

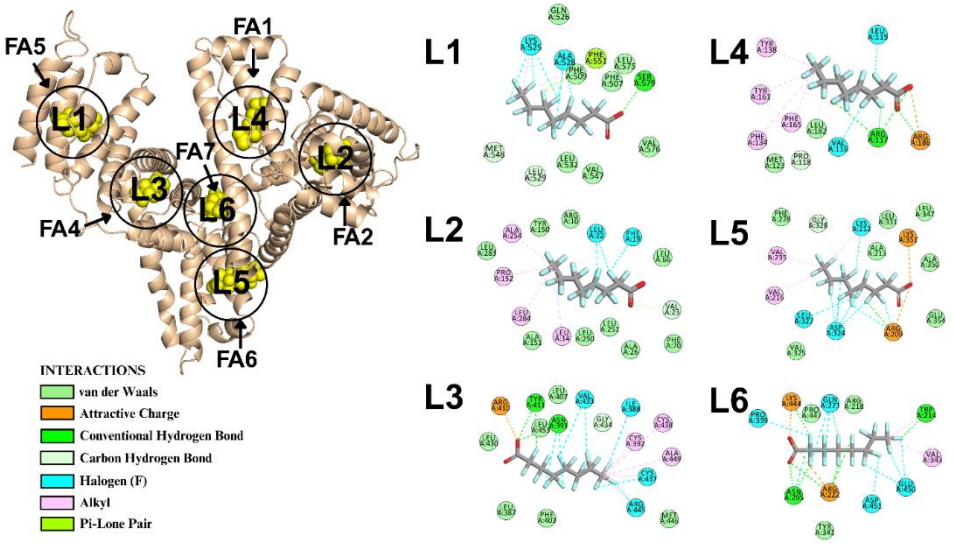

Fig. 1. Left: 3D structure of HSA with PFOA bound at the six top-scoring docking positions. Right: 2D interaction diagrams between HSA residues and PFOA for these positions.

A binding site with a calculated binding score of –37.66 kJ/mol was identified in domain Ia, near the N-terminus and adjacent to fatty acid binding site 2 (FA2) (Fig. S-1). This site is characterized by a hydrogen bond between Val23 and the carboxylic group of PFOA, supported by additional stabilizing contacts: alkyl interactions with Leu14, Pro152, Ala254 and Leu284; halogen interactions with Leu22 and Phe19; and van der Waals contacts with Arg10, Leu66, Tyr150, Ala151, Leu251 and Leu283 (Fig. 1, L2). Although this binding site has not been previously described, it is occupied by myristic acid in the crystal structure reported by Maso *et al.*[13]

The best-characterized PFOA binding site reported in multiple studies[13,30,31] and identified as a high-affinity site by Maso *et al.*[13] corresponds to the third-

highest affinity pose in our docking simulations (–36.82 kJ/mol). This site is located at Sudlow's site II, overlapping with fatty acid site 4 (FA4, Fig. S-1). At this position, the carboxylic group of PFOA forms a salt bridge with Arg410 and hydrogen bonds with Tyr411 and Asn391, all of which have been consistently identified as key interacting residues in previous reports. Additional stabilization is provided by halogen interactions with Val433, Ile388, Cys437 and Arg445, as well as alkyl interactions with Cys392, Cys438 and Ala449 (Fig. 1, L3).

The fourth-highest affinity PFOA binding site identified in our docking simulations –35.98 kJ/mol) is located at fatty acid site 1 (FA1), a site previously described by Salvalaglio *et al.*[32] and found to be occupied by myristic acid in the crystal structure reported by Maso *et al.*[13] At this location, PFOA binding is primarily mediated through interactions of its carboxylic head group with Arg186 and Arg117. Additional stabilization arises from halogen contacts with Leu115 and Val116, π-alkyl interactions with Phe134, Tyr138, Tyr161 and Phe165, and a carbon–hydrogen bond with Pro118 (Fig. 1, L4).

The next binding site (L5), with a predicted binding energy of –35.15 kJ/mol, aligns with fatty acid site 6 (FA6) and has been previously reported as a lower--affinity site for PFOA[13,33] (Fig. 1, L5). Key stabilizing interactions include salt bridges with Lys351 and Arg209, along with halogen interactions involving Lys212, Asp324 and Leu327. Additional stabilization is provided by alkyl interactions with Val216 and Val235.

The final PFOA binding site previously described in the literature by Maso *et al.*[13] and Crisali *et al.*[30] corresponds to the next-highest affinity pose identified in our docking simulations, with a predicted binding energy of –33.47 kJ/mol. This site is located near fatty acid site 7 (FA7), where the carboxylic head group of PFOA forms salt bridges with Arg222 and Lys444. Binding is further stabilized by halogen interactions with Gln221, Pro339, Glu450 and Asp451; hydrogen bonds with Trp214 and Asn295; and an alkyl interaction with Val343 (Fig. 1, L6). This site has also been observed in crystal structures and characterized as a low-affinity PFOA binding site.[13]

In addition to the previously reported binding sites, our analysis identified six lower-affinity PFOA binding sites, each with predicted binding energies below –33.47 kJ/mol. These sites have not been described in earlier studies. As with the higher-affinity sites, PFOA binding at these locations is stabilized through a combination of salt bridges involving Arg and Lys residues, hydrogen bonds, alkyl interactions, and halogen contacts (Fig. S-2 of the Supplementary material). Among the twelve highest-affinity sites identified in our docking study, only one previously reported lower-affinity site, located at a cleft in the crystal structure, was not observed. This absence is likely attributable to the high conformational mobility at the interface between domains, which may preclude stable ligand binding at this position.

To further explore the stability and temporal behavior of these interactions under dynamic conditions, we monitored PFOA–HSA contacts throughout the MD simulations. During the simulation, no significant conformational changes in the protein structure were observed, with the *RMSD* remaining within 3 Å throughout the entire trajectory (Figs. S-3 and S-4 of the Supplementary material). For this purpose, PLIP (protein ligand interaction profiler)[34] program was used for identification of ligand–residue interactions in each MD frame. These data are further used for generation of ligand–residue interaction maps (LRIMs) for all 12 binding positions across all three simulation replicas (Fig. 2). These maps show the number of frames in which each amino acid of HSA interacts with the corresponding ligand. Peak height reflects the number of frames with interaction, while the vertical spacing between the lines represents different ligand positions within a single simulation and is scaled to 30 % of the total simulation time. Multiple simultaneous interactions between a single ligand and the same amino acid are possible and are captured in the diagrams.

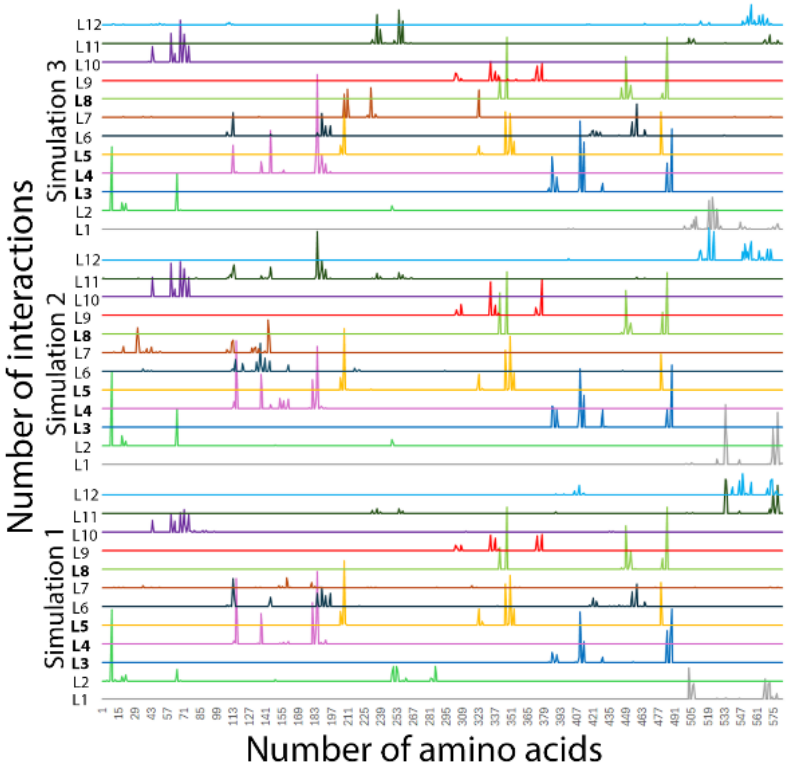

Fig. 2. Ligand–residue interaction maps (LRIMs) for ligands L1–L12 from three MD simulations. The *x*-axis shows amino acid positions, the *y*-axis the number of frames with contacts. Different colors mark individual ligands; peaks indicate residues frequently involved in binding.

Strongly bound ligands were defined using two criteria: 1) the ligand remained bound to the same site throughout all three simulations and 2) the ligand formed interactions with at least three different HSA amino acids for more than 50 % of the total simulation time. Applying these criteria yielded four binding sites corresponding to positions L3, L4, L5 and L8 from the docking study (Table I). Position L3 corresponds to the high-affinity site identified in crystallographic studies of HSA with PFOA and myristic acid, located at Sudlow's site II (FA4). Positions L4 and L5 correspond to FA1 and FA6, respectively; in the crystallographic study, FA1 was occupied by myristic acid, whereas FA6 was occupied by PFOA. Position L8 has not been previously reported as a PFOA binding site but corresponds to the FA3 site and it is also occupied with myristic acid in the crystal structure. Furthermore, the FA3 site is situated near Sudlow's site II.

To assess potential changes in ligand binding positions or orientations during simulations, *RMSD* values were calculated and *RMSD* plots were generated for all three simulations over the 1,000-ns interval. *RMSD* plots show that PFOA at positions L3 (FA4) and L8 (FA3) remain in the same orientation within the binding site thorough the simulation time with small *RMSD* values around 2 Å. However, a slight change in the orientation of the ligand at position L3 (FA4) was detected in one of the three simulations after 350 ns, as shown in Fig. 3. As noted previously, position L3 (FA4) is located at Sudlow's site II and lies in close proximity to position L8 (FA3). These two sites share a stabilizing residue, Arg485. The observed change in ligand orientation at position L3 (FA4), previously characterized as the highest-affinity PFOA binding site, is corelated to a conformational change of Arg485 side chain, which interacts with ligands at both positions in our simulations. In contrast, the binding at positions L4 (FA1) and L5 (FA6) shows higher *RMSD* values of around 5–8 Å, indicating more disordered binding sites and more conformational freedom for the ligand. Overall, the *RMSD* results support the conclusion that all four binding sites identified from the interaction diagrams are stable PFOA binding sites. RMSD profiles for all other ligand positions are provided in Fig. S-5 of the Supplementary material.

To further validate whether the four sites identified in our MD analysis represent true PFOA binding positions on HSA in the absence of competing ligands, we calculated binding free energies for all 12 positions using the MM-PBSA method (Table I). The calculated binding energy for position L3 (FA4), previously reported as the highest-affinity PFOA site, was below –62.76 kJ/mol, indicating very strong ligand binding. The binding energy for position L5 (FA6), described in earlier studies as a low-affinity PFOA site, was approximately 20.92 kJ/mol less favorable than position L3 (FA4), consistent with previous reports showing PFOA binding to both sites but with higher affinity at position L3 (FA4). In contrast, binding energies for positions L4 (FA1) and L8 (FA3) were more than 20.92 and

83.68 kJ/mol lower (*i.e.*, more favorable) than that of position L3 (FA4), respectively. Although crystallographic data indicate that myristic acid binds more strongly than PFOA at these sites, our results suggest that, in the absence of myristic acid, PFOA binding at FA1 (position L4) and FA3 (position L8) is actually stronger than at FA4 (position L3). MM-PBSA-calculated binding energies for PFOA at other eight positions are substantially lower; however, there are still indications that PFOA may bind at two additional positions: FA5 (position L1) and FA2 (position L2). Discrepancies between docking scores and MM-PBSA results, such as the case of L8 (FA3), highlight the limited predictive power of docking alone. Docking employs simplified scoring functions and rigid structures, whereas MD simulations with MM-PBSA incorporate conformational flexibility and dynamic interactions, offering a more reliable estimate of binding affinities.

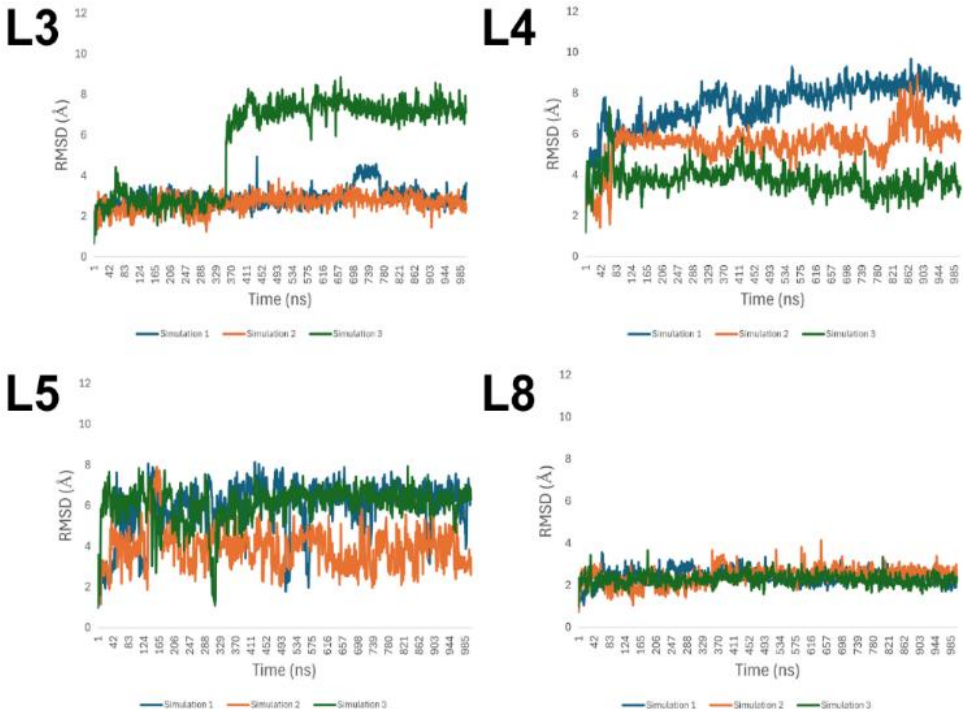

Fig. 3. RMSD plots for the four ligands of interest (L3, L4, L5 and L8) during 1,000-ns MD simulations.

Based on the combined analysis of MD trajectories, protein–ligand interaction profiles, *RMSD* values, and MM-PBSA-calculated binding energies, we conclude that, in the absence of competing ligands, PFOA preferentially binds to the four proposed binding sites. To further characterize these interactions, free-energy landscapes were constructed for ligands at each of these positions. The free energy

landscape for PFOA binding at position L8 (FA3) exhibits a well-defined single minimum, indicating a stable binding mode. In contrast, the landscape at position L3 (FA4) reveals two distinct minima, which arise from conformational changes of Arg485. These observations are in agreement with both the *RMSD* profiles and the calculated MM-PBSA binding energies. Conversely, the landscapes corresponding to positions L4 (FA1) and L5 (FA6) display more diffuse minima, consistent with their higher *RMSD* fluctuations and visual inspection of the MD trajectories (Fig. 4).

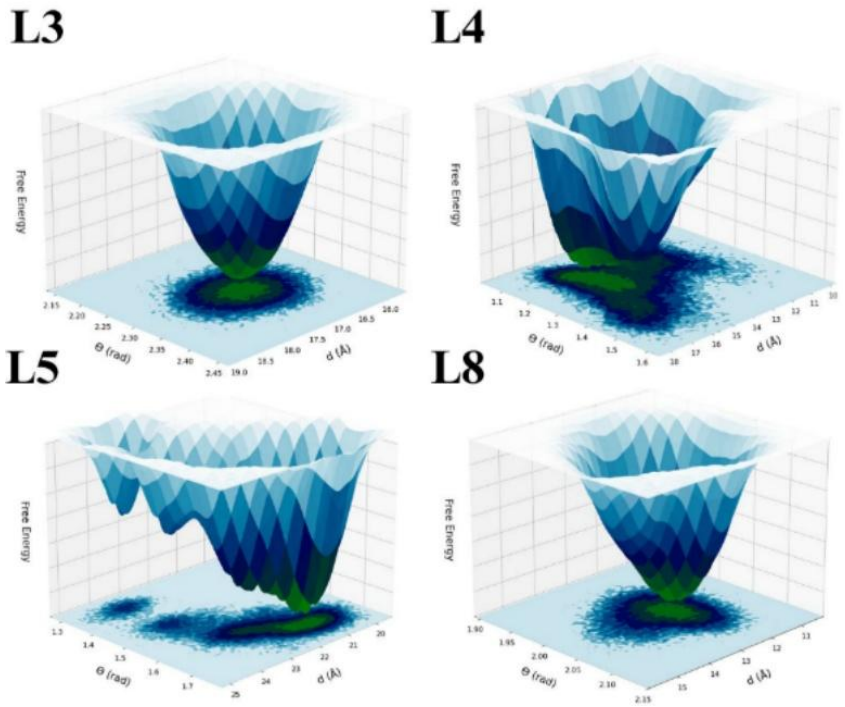

Fig. 4. Free-energy landscapes for best binding ligands (L3, L4, L5, L8).

To further characterize the molecular determinants of PFOA binding at the four identified sites, we employed the PLIP program[34] to track all protein–ligand interactions over the full MD trajectories. This analysis enables the identification of critical HSA residues involved in stabilizing PFOA at each site. Using these data, we constructed interaction diagrams illustrating the residues engaged in binding and the corresponding interaction types throughout the 1,000-ns simulations, including only those residues that interact with the ligand for more than 40 % of the simulation time (Fig. 5).

Our analysis shows that PFOA binding at the site with the most favorable MM-PBSA-calculated binding energy (FA3, L8) is primarily stabilized by two salt bridges formed with Arg347 and Arg485, both present in every frame of the 1,000-

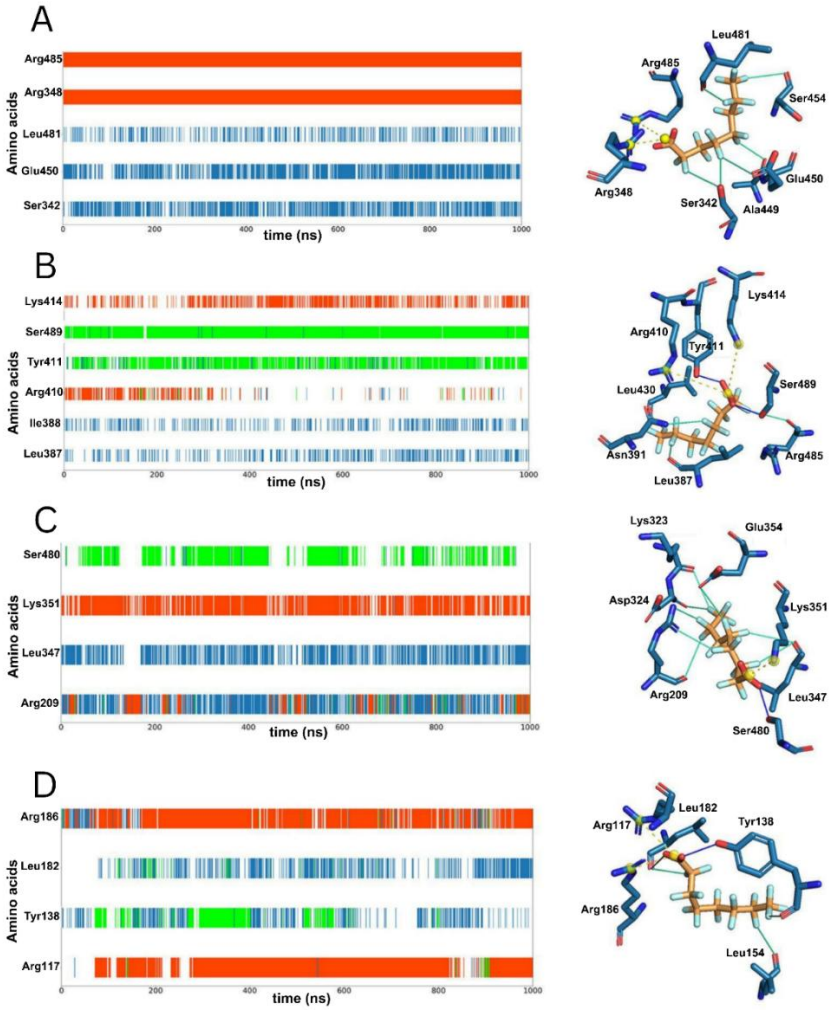

Fig. 5. Interactions formed by specific amino acid residues at the four identified PFOA binding sites on HSA. Panels A–D correspond to the key residues involved in binding L8, L3, L4 and L5, respectively. Left: interactions between protein residues and PFOA observed in at least 40 % of the 1,000-ns MD simulations. Orange bars indicate salt bridges, blue bars indicate halogen interactions, and green bars indicate hydrogen bonds. Right: three-dimensional representations of PFOA bound at each site, showing the interacting HSA residues.

-ns simulations. Additional stabilization is provided by halogen interactions with Ser342, Glu450 and Leu481 (Fig. 5A). Binding at the FA4 (L3) site is mediated

by a salt bridge with either Arg410 at the start of the simulation or Lys414, located in close proximity, later in the trajectory. This site also features two hydrogen bonds with Tyr411 and Ser489 curtail for stabilization of carboxylic group, as well as halogen interactions with Leu387 and Ile388 (Fig. 5B). At L4 position (FA6), the carboxyl group of PFOA is anchored by a persistent salt bridge with Lys351 and either an alternating hydrogen bond with Ser480 or a salt bridge with Arg209; when Ser480 forms a hydrogen bond, Arg209 predominantly engages in halogen interactions (Fig. 5C). Finally, the binding at L5 (FA1) is characterized by two salt bridges formed with Arg117 and Arg185, along with alternating halogen and hydrogen bond interactions involving Tyr138 and Leu182 (Fig. 5D).

CONCLUSION

In this study, we combined molecular docking with extensive molecular dynamics (MD) simulations to comprehensively map potential PFOA binding sites on human serum albumin (HSA). While previous crystallographic analyses in the presence of myristic acid identified one high-affinity and three low-affinity binding sites, our approach revealed twelve distinct binding poses, including six that have not been previously reported. Through ligand-residue interaction mapping, RMSD analysis, and MM-PBSA free energy calculations, we identified four binding sites (FA3 (L8), FA4 (L3), FA1 (L4) and FA6 (L5)) as the most likely PFOA binding positions in the absence of competing ligands.

Our simulations show that PFOA binding is stabilized by persistent salt bridges and hydrogen bonds between the carboxylic head group and protein residues, as well as halogen contacts between the PFOA tail and protein amino acids. Among the identified sites, FA3 (L8) exhibited the most favorable calculated binding energy. Notably, our results suggest that FA1 (L4) and FA3 (L8) may bind PFOA more strongly than the well-characterized FA4 (L3) site in the absence of myristic acid. The free-energy landscapes further confirmed the stability of PFOA at these sites, revealing well-defined minima at FA3 (L8) site, consistent with strong binding.

By integrating MD simulations with docking predictions, this work advances the current understanding of PFOA-HSA interactions beyond static structural models. These findings provide a more complete picture of the binding landscape, which can inform the rational design of biomimetic capture agents and guide strategies for environmental remediation. Future experimental validation of these predicted sites and binding affinities, such as site-directed mutagenesis of FA1/ /FA3 residues or by ITC and fluorescence displacement assays in the presence and absence myristic acid, will be essential to translate these computational insights into practical applications for PFOA detection and removal.

SUPPLEMENTARY MATERIAL

Additional data and information are available electronically at the pages of journal website: https://www.shd-pub.org.rs/index.php/JSCS/article/view/13509, or from the corresponding author on request.

Acknowledgements. This research was supported by the Science Fund of the Republic of Serbia, grant no. 7750288, "Tailoring Molecular Magnets and Catalysts Based on Transition Metal Complexes – TMMagCat". We also acknowledge the support of the Ministry of Science, Technological Development and Innovation of the Republic of Serbia (Contract Nos. 451-03-136/2025-03/200168 and 451-03-136/2025-03/200026).

ИЗВОД

МЕТОДОЛОШКИ ПРИСТУП ЗАСНОВАН НА МОЛЕКУЛСКОДИНАМИЧКИМ СИМУЛАЦИЈАМА ЗА ПОЈАШЊЕЊЕ МЕСТА ВЕЗИВАЊА PFOA НА HSA

АЛЕКСАНДРА М. ЂУРЂЕВИЋ ЂЕЛМАШ[1], ДАНИЛО ТРАЈКОВИЋ[1], КАРЛА МИЛЧИЋ[2] и МИЛОШ МИЛЧИЋ[1]

[1]Универзитет у Београду – Хемијски факултет, Студентски трг 12–16, 11158Београд и [2]Институт за хемију, технологију и металургију, Центар за хемију, Универзитет у Београду, Институт од националног значаја за Републику Србију, Његошева 12, 11000 Београд

Перфлуорооктаноична киселина (PFOA) је постојани загађивач животне средине који се снажно везује за хумани серумски албумин (HSA), утичући на њену дистрибуцију и токсикокинетику. Иако су кристалографске студије у присуству миристинске киселине идентификовале ограничен број везивних места високог афинитета, додатна места могу остати неоткривена због компететивног везивања. У овом раду смо комбиновали молекулско доковање високе резолуције са обимним симулацијама молекулске динамике (MD) како бисмо свеобухватно окарактерисали интеракције PFOA–HSA. Приступ са подељеним мрежама открио је дванаест непоклапајућих везивних позиција, укључујући шест претходно непознатих. Анализа интеракција лиганда и амино-киселина, *RMSD* анализа и прорачуни слободне енергије везивања методом MM/PBSA идентификовали су четири места, FA3, FA4, ФА1 и FA6, као најстабилнија везивна места PFOA у одсуству конкурентних лиганада. Међу њима, FA3 је показало најповољнију израчунату енергију везивања, док су FA1 и FA3 показала јаче везивање од добро окарактерисаног FA4 места у условима без миристинске киселине. Перзистентни сони мостови, водоничне везе и халогене интеракције идентификовани су као кључне стабилизујуће интеракције. Анализа енергетских пејзажа додатно је потврдила стабилност везивања PFOA на овим местима. Ови резултати пружају потпунији увид у везивни пејзаж PFOA на HSA и могу послужити као основа за дизајн биомиметичких хватача и развој стратегија за ремедијацију животне средине.

(Примљено 20. августа, ревидирано 27. августа, прихваћено 5. септембра 2025)

REFERENCES

1. X. Du, Y. Li, Y. L. Xia, S. M. Ai, J. Liang, P. Sang, X. L. Ji, S. Q. Liu, *Int. J. Mol. Sci.* **17** (2016) 144 (https://doi.org/10.3390/ijms17020144)
2. J. Kraut, *Science* **242** (1988) 533 (https://doi.org/10.1126/science.3051385)
3. D. B. Roche, S. J. Tetchner, L. J. McGuffin, *BMC Bioinformatics* **12** (2011) (https://doi.org/10.1186/1471-2105-12-160)

4. I. D. Kuntz, K. Chen, K. A. Sharp, P. A. Kollman, *PNAS* **96** (1999) 9997 (https://doi.org/10.1073/pnas.96.18.9997)
5. K. Henzler-Wildman, D. Kern, *Nature* **450** (2007) 964 (https://doi.org/10.1038/nature06522)
6. M. Held, P. Metzner, J. H. Prinz, F. Noé, *Biophys. J.* **100** (2011) 701 (https://doi.org/10.1016/j.bpj.2010.12.3699)
7. D. B. Roche, M. T. Buenavista, L. J. McGuffin, *PLoS One* **7** (2012) (https://doi.org/10.1371/journal.pone.0038219)
8. G. Fanali, A. Di Masi, V. Trezza, M. Marino, M. Fasano, P. Ascenzi, *Mol. Aspects Med.* **33** (2012) 209 (https://doi.org/10.1016/j.mam.2011.12.002)
9. S. Wang, S. Liu, Y. Zhang, J. He, D. H. Coy, L. Sun, *Health Sci. J.* **14** (2020) 698 (https://www.itmedicalteam.pl/articles/human-serum-albumin-hsa-and-itsapplications-as-a-drug-delivery-vehicle.pdf)
10. M. Forsthuber, A. M. Kaiser, S. Granitzer, I. Hassl, M. Hengstschläger, H. Stangl, C. Gundacker, *Environ. Int.* **137** (2020) 105324 (https://doi.org/10.1016/j.envint.2019.105324)
11. K. Li, P. Gao, P. Xiang, X. Zhang, X. Cui, L. Q. Ma, *Environ. Int.* **99** (2017) 43 (https://doi.org/10.1016/j.envint.2016.11.014)
12. K. Steenland, T. Fletcher, D. A. Savitz, *Environ. Health Perspect.* **118** (2010) 1100 (https://doi.org/10.1289/ehp.0901827)
13. L. Maso, M. Trande, S. Liberi, G. Moro, E. Daems, S. Linciano, F. Sobott, S. Covaceuszach, A. Cassetta, S. Fasolato, L. M. Moretto, K. De Wael, L. Cendron, A. Angelini, *Prot. Sci.* **30** (2021) 830 (https://doi.org/10.1002/pro.4036)
14. G. Moro, S. Liberi, F. Vascon, S. Linciano, S. De Felice, S. Fasolato, C. Foresta, L. De Toni, A. Di Nisio, L. Cendron, A. Angelini, *Chem. Res. Toxicol.* **35** (2022) 2049 (https://doi.org/10.1021/acs.chemrestox.2c00211)
15. M. Peng, Y. Xu, Y. Wu, X. Cai, W. Zhang, L. Zheng, E. Du, J. Fu, *Toxics* **12** (2024) 43 (https://doi.org/10.3390/toxics12010043)
16. Y.-D. Yang, N. Lu, R. Tian, *Int. J. Biol. Macromol.* **254** (2024) 128069 (https://doi.org/10.1016/j.ijbiomac.2023.128069)
17. J. Fan, A. Fu, L. Zhang, *Quant. Biol.* **7** (2019) 83 (https://doi.org/10.1007/s40484-019-0172-y)
18. V. Limongelli, *Wiley Interdiscip. Rev. Comput. Mol. Sci.* **10** (2020) e1455 (https://doi.org/10.1002/wcms.1455)
19. R. Anandakrishnan, B. Aguilar, A. V. Onufriev, *Nucleic Acids Res.* **40** (2012) W537 (https://doi.org/10.1093/nar/gks375)
20. G. M. Morris, H. Ruth, W. Lindstrom, M. F. Sanner, R. K. Belew, D. S. Goodsell, A. J. Olson, *J. Comput. Chem.* **30** (2009) 2785 (https://doi.org/10.1002/jcc.21256)
21. Gaussian, Inc., Wallingford, CT, 2016 (https://gaussian.com/citation/)
22. O. Trott, A. J. Olson, *J. Comput. Chem.* **31** (2010) 455 (https://doi.org/10.1002/jcc.21334)
23. C. Tian, K. Kasavajhala, K. A. A. Belfon, L. Raguette, H. Huang, A. N. Migues, J. Bickel, Y. Wang, J. Pincay, Q. Wu, C. Simmerling, *J. Chem. Theory. Comput.* **16** (2020) 528 (https://doi.org/10.1021/acs.jctc.9b00591)
24. J. Wang, R. M. Wolf, J. W. Caldwell, P. A. Kollman, D. A. Case, *J. Comput. Chem.* **25** (2004) 1157 (https://doi.org/10.1002/jcc.20035)
25. C. I. Bayly, P. Cieplak, W. D. Cornell, P. A. Kollman, *J. Phys. Chem.* **97** (1993) 10296 (https://doi.org/10.1021/j100142a004)

26. D. R. Roe, B. R. Brooks, *J. Chem. Phys.* **153** (2020) 054123 (https://doi.org/10.1063/5.0013849)
27. M. J. Abraham, T. Murtola, R. Schulz, S. Páll, J. C. Smith, B. Hess, E. Lindahl, *SoftwareX* **1**–**2** (2015) 19 (https://doi.org/10.1016/j.softx.2015.06.001)
28. A. Đurđević Đelmaš, T. Šeba, N. Gligorijević, M. Pavlović, M. Gruden, M. Nikolić, K. Milcic, M. Milčić, *Int. J. Biol. Macromol.* **306** (2025) 141425 (https://doi.org/10.1016/j.ijbiomac.2025.141425)
29. Y. Wu, J. Bao, Y. Liu, X. Wang, X. Lu, K. Wang, *Toxics* **12** (2024) 46 (https://doi.org/10.3390/toxics12010046)
30. A. M. Crisalli, A. Cai, B. P. Cho, *Chem. Res. Toxicol.* **36** (2023) 703 (https://doi.org/10.1021/acs.chemrestox.3c00011)
31. G. A. Tiburtini, L. Bertarini, M. Bersani, T. A. Dragani, B. Rolando, A. Binello, A. Barge, F. Spyrakis, *Arch. Toxicol.* **98** (2024) 3035 (https://doi.org/10.1007/s00204-024-03797-0)
32. M. Salvalaglio, I. Muscionico, C. Cavallotti, *J. Phy. Chem., B* **114** (2010) 14860 (https://doi.org/10.1021/jp106584b)
33. H. Chen, Q. Wang, Y. Cai, R. Yuan, F. Wang, B. Zhou, *Int. J. Environ. Res. Public Health* **17** (2020) 1319 (https://doi.org/10.3390/ijerph17041319)
34. S. Salentin, S. Schreiber, V. J. Haupt, M. F. Adasme, M. Schroeder, *Nucleic Acids Res.* **43** (2015) W443 (https://doi.org/10.1093/nar/gkv315).